7

Hydrogeological flow logging and dye tracer tests on the Hydrogeological Experimental Site of Poitiers University (France)

A. Boulais, T. Gaillard and H. Geairon

Introduction

Karst may be defined as a network of conduits that enable groundwater transfer. Conduit dimensions range from centimetres to meters. Karst systems are organized around the connectivity of different types of voids: the primary porosity of the host rock, fissure porosity, and dissolution voids produced by karstification of carbonates.

At the regional scale, karst voids are typically smaller in volume than fissures and pores. Mangin (1975), based on drainage analyses of systems studied at the Moulis laboratory (France), concluded that karst voids account for only a very small fraction of the limestone massif—on the order of 0.2%. This estimate has been supported by data from various karst systems compiled by Worthington (2003).

DOI: https://doi.org/10.1051/978-2-7598-3934-6.c007

The spatial distribution of karst conduits is only partially known, generally at locations where they intersect the land surface (e.g., sinkholes and springs) or are intercepted by boreholes. Even when accessible portions of a karst system can be mapped by speleologists, the explored conduits represent only a small fraction of the full drainage network.

Research at the Hydrogeological Experimental Site (HES) of Poitiers University (France), focuses on a limestone aquifer located at depths of approximately 35–130 m (supra-Toarcian aquifer). The site comprises 45 boreholes over an area of 15 ha, including 28 boreholes concentrated within a 210 × 210 m square (Fig. 1).

Karst features at the site occur preferentially within four lithostratigraphic units, each sub-horizontal, 2–5 m thick, and located at depths of ~30, 50, 85, and 115 m below ground surface (Mari and Porel, 2008; Mari et al., 2009; Mari and Porel, 2024).

A 3D seismic survey was conducted at the HES in 2004. Complementary to the surface seismic data, full acoustic logs were acquired in 6 boreholes: C1, MP5, MP6, M08, and M09. Cross-analysis of the 3D seismic model and borehole logs revealed a strong relationship between low-velocity seismic zones and inflow/outflow horizons associated with high hydraulic conductivity (Mari and Porel, 2008).

Finally, using tracer-test data from 50 inter-well tests performed within the seismic survey area, together with borehole flowmeter logs, Bodin et al. (2022) demonstrated the feasibility of delineating discrete karst conduit networks.

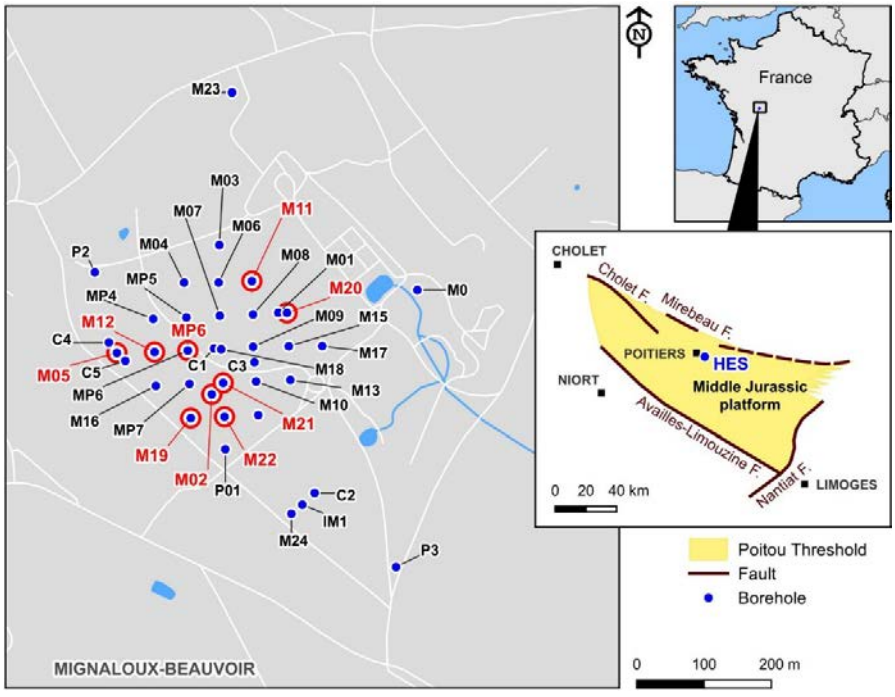

Figure 1 *Location of the boreholes at the HES in Poitiers, France.*

The value of borehole logging for aquifer characterization has been demonstrated by several authors (Keys, 1990; Paillet, 1993; US National Research Council, 1996; Paillet and Reese, 2000; Muldoon et al., 2001; Schürch and Buckley, 2002; Williams et al., 2002; Audouin et al., 2008). At the HES, geophysical borehole investigations have included caliper, natural gamma, electrical logs, flow logs, borehole imaging (Optical Televiewer - OPTV), and heat-pulse flowmeter surveys. All resulting data are publicly available via the "H+" database, developed within the framework of the Environmental Research Observatory (ERO) program.

Two categories of information have been derived from borehole logging: (1) the geological structure of the aquifer, and (2) the structure of the flow paths. Electrical, natural gamma-ray, and borehole imaging logs have been applied both to identify lithologic variations and to correlate stratigraphic units between boreholes (Gaillard et al., 2024).

Remote pumping logs revealed both upward and downward flows within the same boreholes during pumping tests. In 2021, tracer tests were performed to confirm these flow patterns in several wells, specifically M02, M05, MP6, M12, M19, and M21.

This paper presents the results of experiments conducted in collaboration with the University of Poitiers team in 2021. It builds upon the findings previously obtained at the site, which were used to define the operational methodology for the 2021 investigations.

Borehole flow logging acquisition

Principle of flow logging

The principle of borehole logging consists of lowering probes or measuring devices into the borehole, connected by a cable that ensures both electrical and mechanical linkage to surface instruments (Fig. 2). These tools continuously record physical or chemical parameters as a function of depth. In flow logging, the instruments measure the velocity and/or quality of moving fluids (e.g., water temperature and electrical conductivity).

At the HES, logging was conducted using a GFTC probe to measure natural Gamma-ray, Flow, Temperature, and electrical Conductivity. The micro-mill tool, equipped with an impeller, records the vertical velocity of water movement within the borehole. This allows identification and quantification of water inflows by detecting variations in fluid velocity along the borehole depth.

Flow logging can be performed under three conditions: (i) without pumping (ambient regime), (ii) with pumping in the borehole being logged (dynamic regime), and (iii) with pumping in an adjacent borehole (cross-dynamic regime), enabling detection of both upward and downward flows.

However, logging results may be disturbed by borehole casings or changes in borehole diameter, which can mask certain inflows. For instance, water moving through a reduced-diameter casing produces artificially elevated flow velocities that are not always associated with natural inflows.

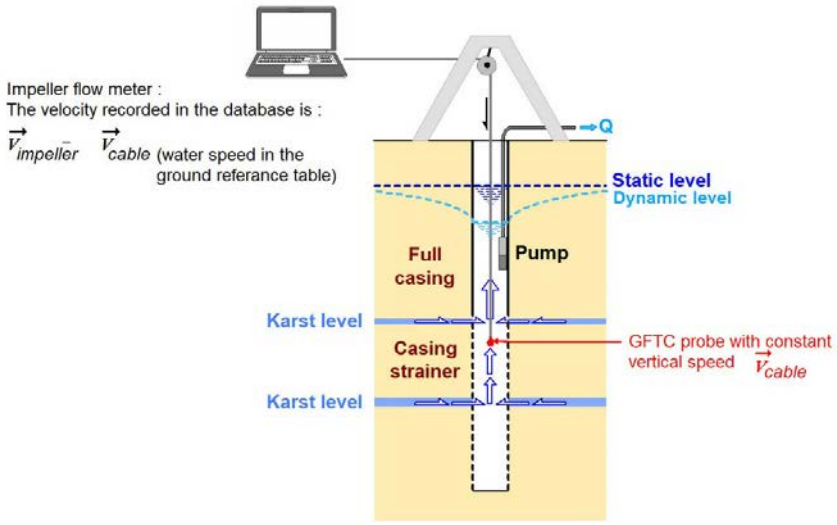

Figure 2 *Schematic diagram of flow logging.*

Downflow and upflow in the borehole

To obtain a complete picture of borehole flow, two recording passes are typically performed:

– downhole pass: The tool is lowered into the borehole, recording data continuously;
– uphole pass: Once at the bottom, the tool is raised while recording data.

When the tool moves with the flow, its velocity is added to that of the fluid. Conversely, when the tool moves against the flow, its velocity is subtracted from that of the fluid (or, if the flow is stronger than the tool's movement, the fluid velocity is subtracted from the tool's velocity). By knowing the downhole and uphole velocities of the tool (measured in a logger linked with a computer), it is possible to correct the micro-current meter readings to obtain the true fluid velocity and its direction of movement in the borehole.

Following the recommendations of Keys (1990), logging was performed during downward passes at a low speed (6 m/min) to minimize disturbance of the water column.

The data under study concern the velocities (in m/mn) and the temperatures (in degrees Celsius).

Dynamic flow logging

The flow logs presented in Figures 3 to 10 allow the identification of water inlets corresponding to productive karst levels. Since the pump is positioned above the probe, only upward flows are measured. The GFTC probe is positioned at the bottom of the borehole and recording is performed by lifting the tool. Water entering the borehole thus causes an increase in velocity measured in rounds per second (rps).

Borehole M05 (Fig. 3) is cased with PVC slotted screens oriented horizontally. The temperature log indicates that groundwater is cooler at 120 m depth (12.70 °C) than at 30 m depth near the surface (12.87 °C). Consequently, the geothermal gradient cannot account for this observation, and the presence of a cooler inflow around 120 m depth is confirmed by the flow log between 110 and 120 m. The velocity derivative shows that no additional flow disturbs the measurement down to 72–76 m, where the signal is perturbed on the derivative (variation in well radius?). Between 32-34 m a typical inflow is detected on the derivative curve.

Borehole MP6B is uncased, and therefore the measurement is not affected by the presence of a screen (Fig. 4). On the temperature log, a pronounced inflection at a depth of 84 m indicates an inflow of water, which is confirmed by the flow log, showing two signal variations clearly highlighted by the derivative at depths of 77 m and 83 m. At the bottom of the borehole, the signal becomes more complex, with a decrease in flow velocity associated with vacuoles clearly visible on the OPTV borehole wall imaging. A variation in the diameter of the open hole may account for the velocity decrease observed between 92 and 100 m.

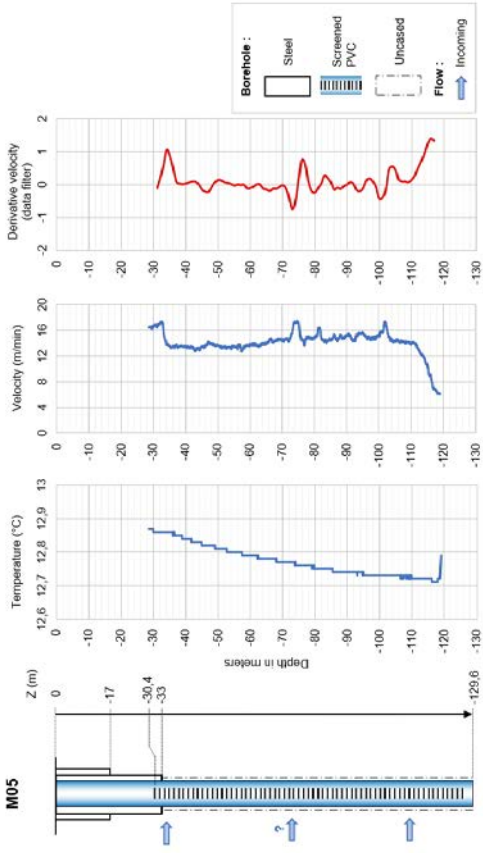

Figure 3 *M05 Flowmeters log with pumping in M05.*

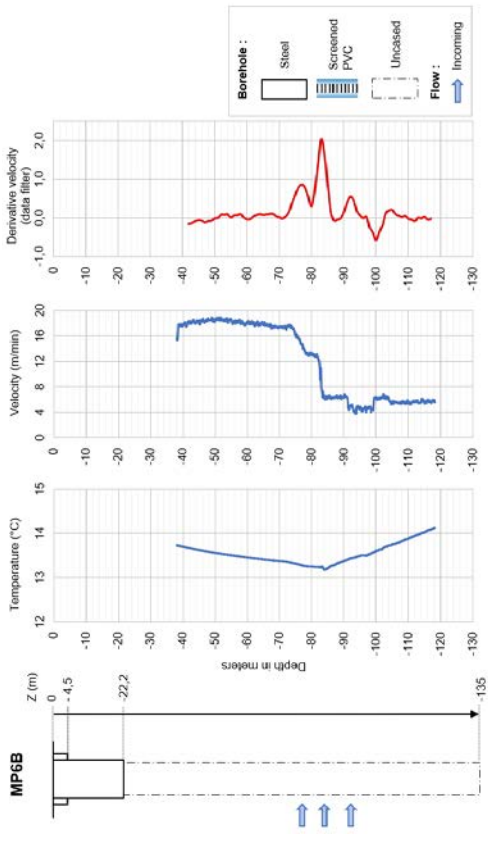

Figure 4 *MP6 Flowmeters log with pumping in MP6.*

The logs from borehole M11 (Fig. 5) are of particular interest because a large cavity encountered between 86.3 and 88.4 m depth results in a significant enlargement of the borehole diameter. In the open-hole section, the temperature log shows two variations at 74 m and 95 m, corresponding to cooler water inflows, but no anomaly is observed within the cavity between 86.3 and 88.4 m. In contrast, the flow log is disturbed between 86 and 88 m due to the enlarged borehole diameter. Water inflows therefore appear to occur around 90–92 m, within a dolomitized and vuggy level, and also between 72 and 74 m, within another dolomitized interval located below a discontinuity.

In borehole M12 (Fig. 6), the logs are affected by the presence of the screen (from 69.9 to 105 m) and by changes in borehole diameter. The temperature log indicates cooler water between 90 and 104 m (13.4 °C). On the flow log, velocity increases at 104 m near the bottom of the screen, an effect attributed to the change in borehole diameter. At the top of the screen, the diameter change also causes a decrease in

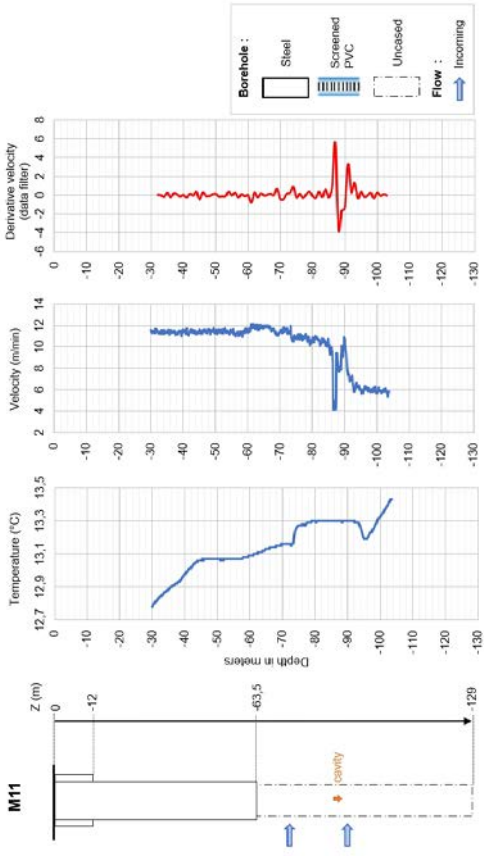

Figure 5 *M11 Flowmeters log with pumping in M11.*

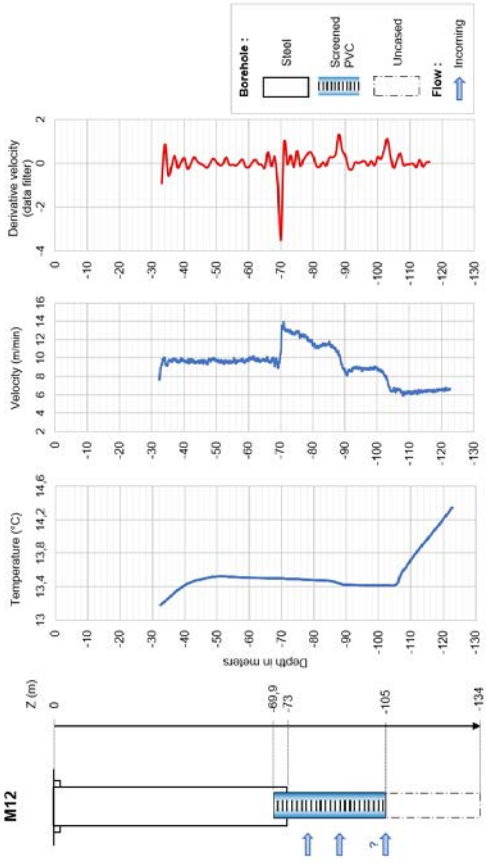

Figure 6 *M12 Flowmeters log with pumping in M12.*

flow velocity. However, between 88 and 90 m depth, a clear water inflow is detected within the screen, confirmed by the flow log. This inflow is also associated with a temperature increase between 86 and 90 m. A second inflow within the screen is identified between 78 and 80 m.

Borehole M19 is fully screened from 75.5 to 133 m depth (Fig. 7). The temperature log provides little information. On the flow log, a water inflow is identified between 116 and 118 m. At 82 m, another inflow causes the velocity to increase (>12 rps), although the transition from PVC screen to steel screen disturbs the measurement.

The logs from borehole M20 (Fig. 8) record a main water inflow, clearly identified on both the temperature log and the flow log, between 86 and 88 m. The velocity derivative is typical of a localized inflow. The geological formation at this depth corresponds to a dolomitized limestone.

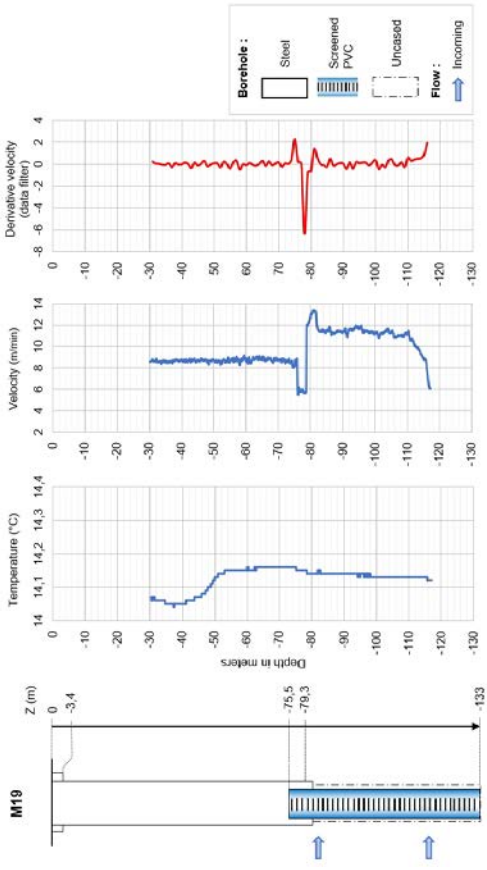

Figure 7 *M19 Flowmeters log with pumping in M19.*

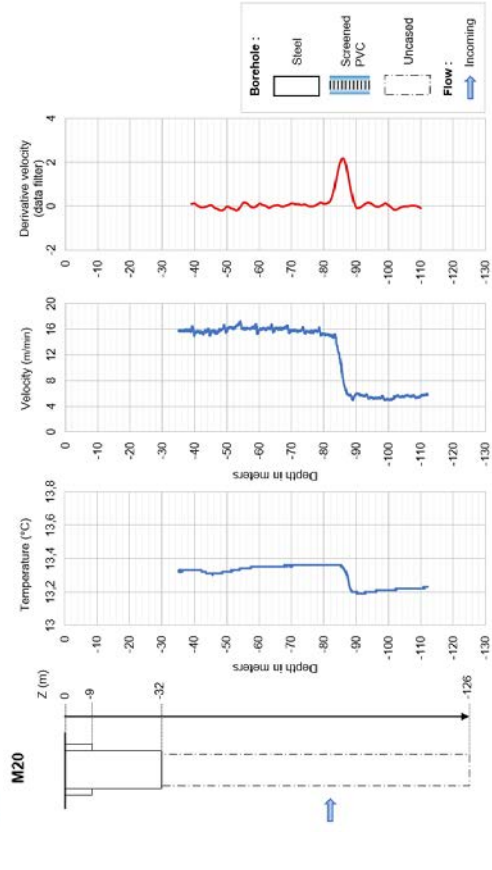

Figure 8 *M20 Flowmeters log with pumping in M20.*

In borehole M21 (Fig. 9), the main water inflow in the open-hole section is located between 91 and 94 m, within a highly dolomitized black limestone. The inflowing water at this depth is cooler (13.6 °C). A minor inflow at 55 m provides an additional contribution to discharge. At the bottom of the screen (68–70 m), the measurement is disturbed.

Finally, Figure 10 presents the measurements from borehole M22. Four successive water inflows are identified, from bottom to top, at approximately 114–116 m, 98–100 m, 84–86 m, and 64–66 m. Unlike the logs from M21 and MP6 (Fig. 4 and 9, respectively), the temperature log shows no distinct anomaly.

In summary, several productive levels (numbered 1 to 10 in Tab. 1) are identified when the flow log is performed under pumping conditions. Comparison of these results with the karst index of Mari and Porel (2024) for boreholes M11, M20, and M21 shows good agreement for levels 3 (64–66 m), 4 (72–74 m),

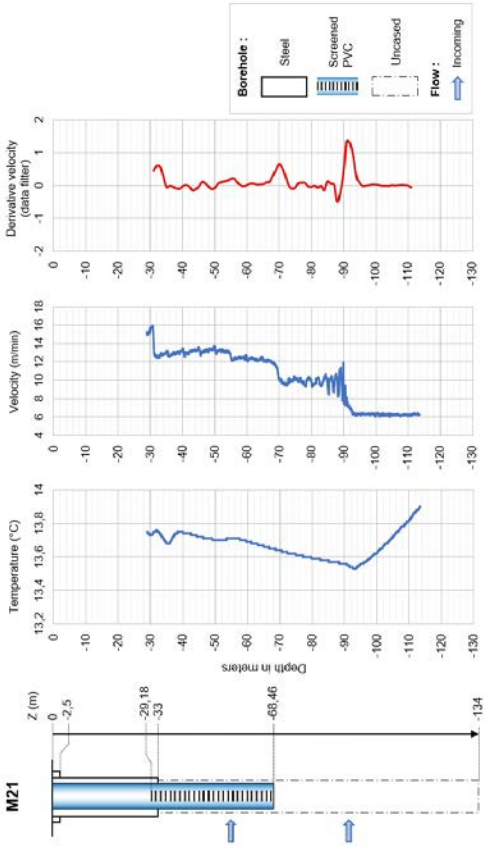

Figure 9 *M21 Flowmeters log with pumping in M21.*

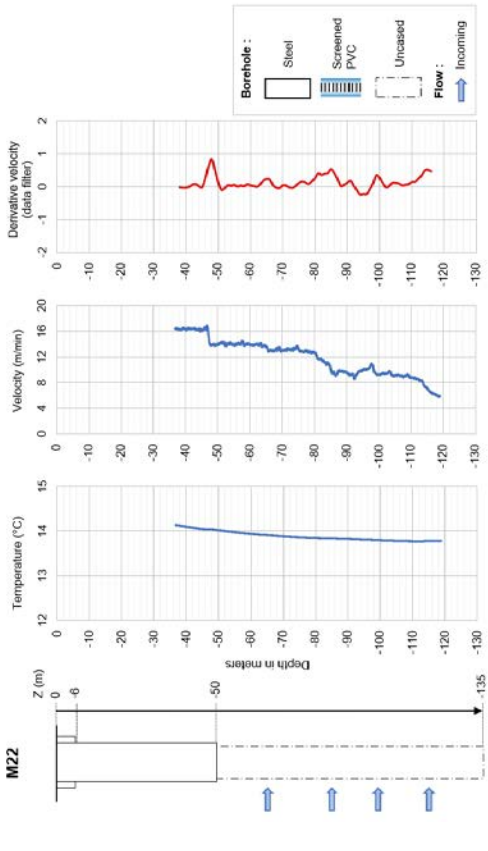

Figure 10 *M22 Flowmeters log with pumping in M22.*

7 (84–88 m), and 10 (114–116 m). They are marked with an asterisk (*) in Table 1. The level that is both the most karstified and the most productive is level 7 (86–88 m). The lithology of this interval corresponds to a dolomitized limestone. The comparison between M21 and M22 provides additional insights. For instance, the karst levels identified by Mari and Porel (2008; 2024) at 100 m (M20) and at 90 m and 110 m (M22) yield only limited water inflows. The lithology of these intervals consists of limestone containing numerous type 1 vacuoles (Gaillard and Moreau, 2026), which appear to be poorly interconnected. Moreover, in M22, the level at 90 m seems to result from the collapse of a dolomitized horizon during drilling.

Table 1 *Locating water inflows into the Supra Toarcian aquifer using temperature and flow logs (in m depth)*

inflow	M05	MP06B	M11	M12	M19	M20	M21	M22
1	32-34							
2							55	
3								**64-66***
4	72-76	77-78	**72-74***					
5		82-84		78-80	80-82			
6								
7			**86-88***	88-90		**86-88***		**84-86***
8		92	**90-92***				91-94	
9								98-100
10	110-120				116-118			114-116
Flow in m3/h	10.6	10.0	10.8	9.8	10.0	10.4	10.1	10.2

Flow logging with pumping in MP6 (crossed dynamics MP6)

Flow logs were carried out on boreholes M02, M05, M12, M19, and M21 with pumping in borehole MP6 at 60 m^3/h. The borehole logs were carried out upwards, at a speed of 6 m/min. Vertical flow velocities are measured, and the velocity derivative is calculated to identify the incoming and outgoing flows from the different karst levels. When velocities decrease, flows in the borehole are downward. Conversely, when velocities increase, flows are upward.

According to the flow log results, upward flows are identified on M02 (Fig. 11) and M12 (Fig. 12), and downward flows are observed on M05 (Fig. 13) and M21 (Fig. 15). Flow directions are uncertain regarding M19 (Fig. 14).

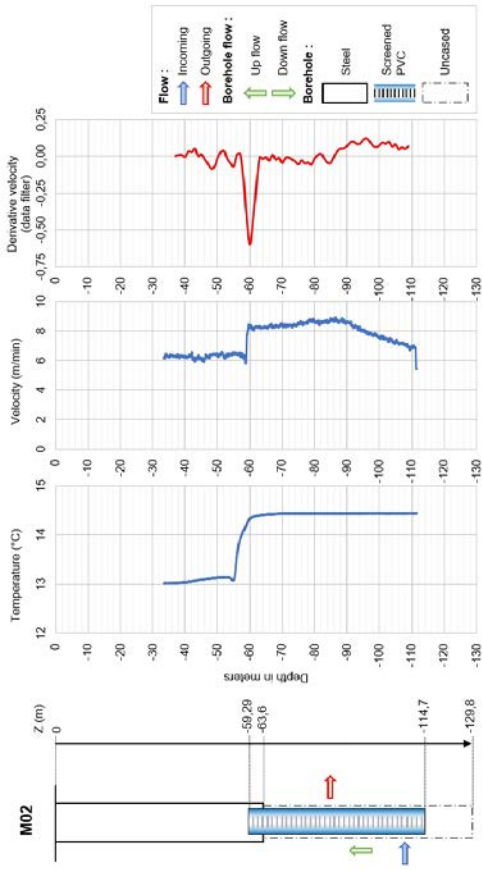

Figure 11 *M02 Flowmeters log - crossed dynamics MP6.*

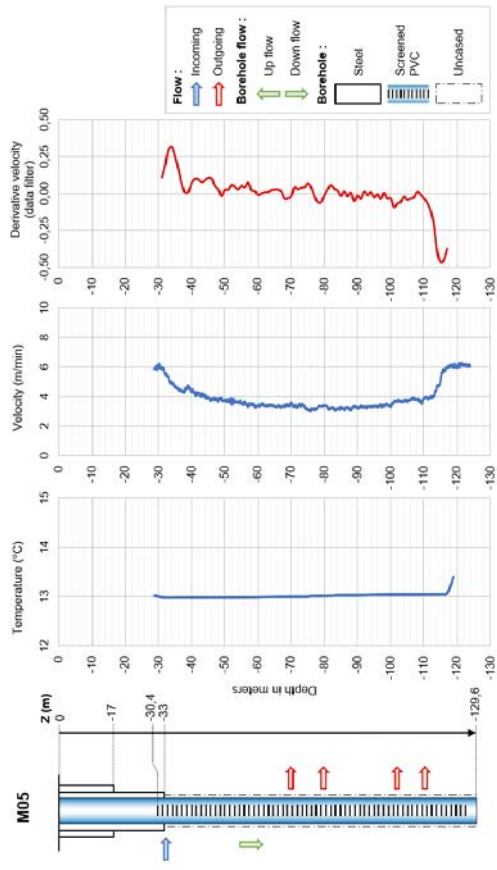

Figure 12 *M05 Flowmeters log - crossed dynamics MP6.*

The productive levels in borehole MP6 are located at depths of 77 m, 83 m, and 92 m (Fig. 4). Considering the spatial distribution of the boreholes (Fig. 1), groundwater flow along the cross-section M05–M12–MP6 follows a complex trajectory. In M05, the productive level at ~35 m is activated and feeds, *per descensum*, the pumped levels in MP6 at 77 m, and in the interval 88 to 92 m, as well as the deeper level at 114 m. In M12, flows converge toward the productive intervals at 78 m and between 80 and 90 m, with part of the discharge also originating from the base of the borehole (104–106 m). Thus, the boreholes alter the natural flow regime by hydraulically connecting multiple porous and/or karstified horizons.

Around boreholes M19, M02, and M21, the flow logs are less contrasted. In M02, the 85–90 m interval is partly supplied by upward flow originating from the 90–110 m level. In M21, the intervals at 70 m and 80–90 m are instead partly fed by flow coming from the 35–60 m level. Once again, the boreholes likely promote mixing between porous and karstified horizons.

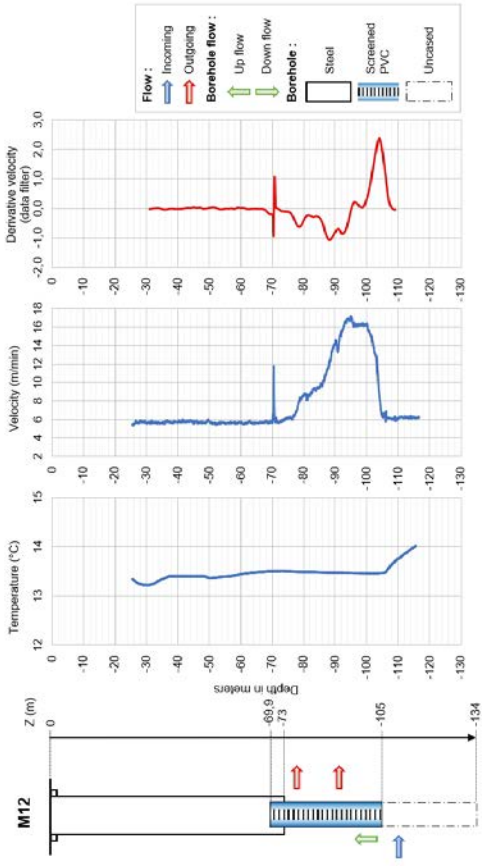

Figure 13 *M12 flowmeters log - crossed dynamics MP6.*

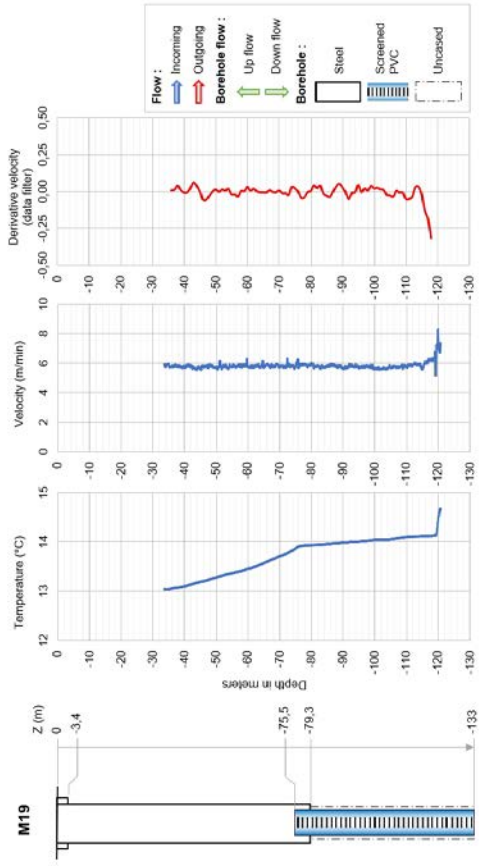

Figure 14 *M19 flowmeters log - crossed dynamics MP6.*

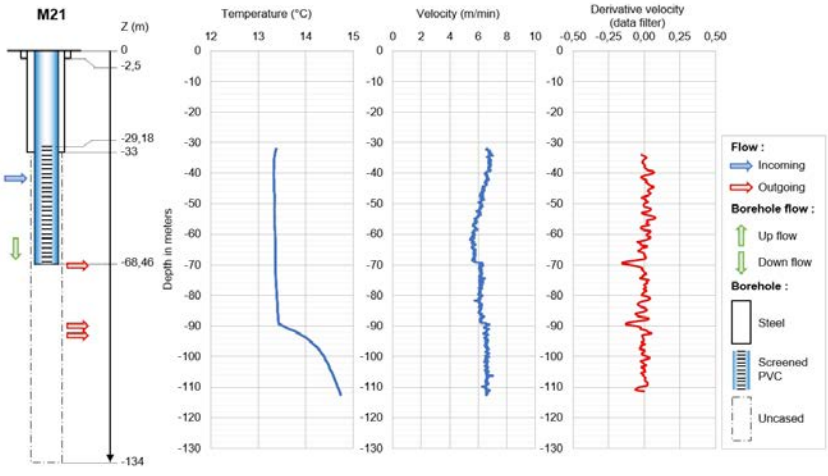

Figure 15 *M21 flowmeters log - crossed dynamics MP6.*

Tracer tests

Tracer test protocol

Tracer tests were conducted to verify mass transfers between the different karst horizons developed in the Supra-Toarcian aquifer. Artificial hydrogeological tracing is an "experimental procedure aimed at making apparent and observable the actual movement of groundwater in an aquifer along one or more defined trajectories between a point of origin and one or more detection points, using an artificial tracer marking the water" (Castany and Margat, 1977, p. 180).

These tests complement those carried out by researchers from the University of Poitiers on other boreholes (see Bodin et al., 2022). The protocol applied in these tests can be summarized as follows (Tab. 2):

1. a pumping operation is launched at a constant flow rate on MP6 until a pseudo-steady flow regime is obtained;
2. the wellbore and tracer injection depth are selected from the results of GFTC logs. The targeted injection depth is generally a few tens of cm upstream of a flow horizon (from the well to the aquifer). The injection boreholes are (Fig. 16):
   - M19 at a depth of 111 m: injection No. 1 on 29/06/2021 at 9:25 a.m. UTC,
   - M19 at a depth of 85 m: injection No. 2 on 01/07/2021 at 1:50 p.m. UTC,
   - M05 at a depth of 111 m: injection No. 3 on 05/07/2021 at 3:40 p.m. UTC;
3. the tracer solution (5 g of uranine diluted in 2 L of water) is injected, followed by rinsing with a volume of 40 L of water. Pipes 2.5 m in length and 1.5 cm in internal diameter are connected down to the targeted injection depth. The total injection time, including rinsing, is less than 3 minutes;
4. tracer migration was monitored at the MP6 pumping borehole outlet pumped at 60 m3/h, using a fluorometer. The fluorometers were positioned at different depths in the observation boreholes M02, M12 and M21 in order to verify the nature of the flows (ascending or descending) between the different karst levels (Tab. 1);
5. the fluorometers used were Valeport Hyperion probes (3) and Albillia GGUN probes (4). The 7 fluorometers were previously calibrated with standard solutions whose concentrations were between 0 µg/L and 999 µg/L.

Results

The Breakthrough Curves (BTC) obtained following the 2 injections carried out on M19 are reported in Figures 17 and 18. The arrival times of the first concentration and the concentration peaks made it possible to better identify an upward flow in the M02 observation borehole and a downward flow in the M21 borehole. The tracer transfer times are longer in the case of the second injection at 85 m depth, which highlights a longer travel distance.

Table 2 *Dye tracer test design.*

Injection borehole	Observation borehole	Fluorometer	
		Depth/ground (m)	Reference fluorometer
M19	M02	62	HYPERION 74041
		85	HYPERION 74039
		100	FL22-243
	M21	65	FL22-241
		85	FL22-242
	MP6	0 (at the outlet of the pumped well)	HYPERION 74040 et FL22-240
M05	M12	76	FL22-242
		85	HYPERION 74041
		100	HYPERION 74039
		105	FL22-241
	MP6	0 (at the outlet of the pumped well)	FL22-239

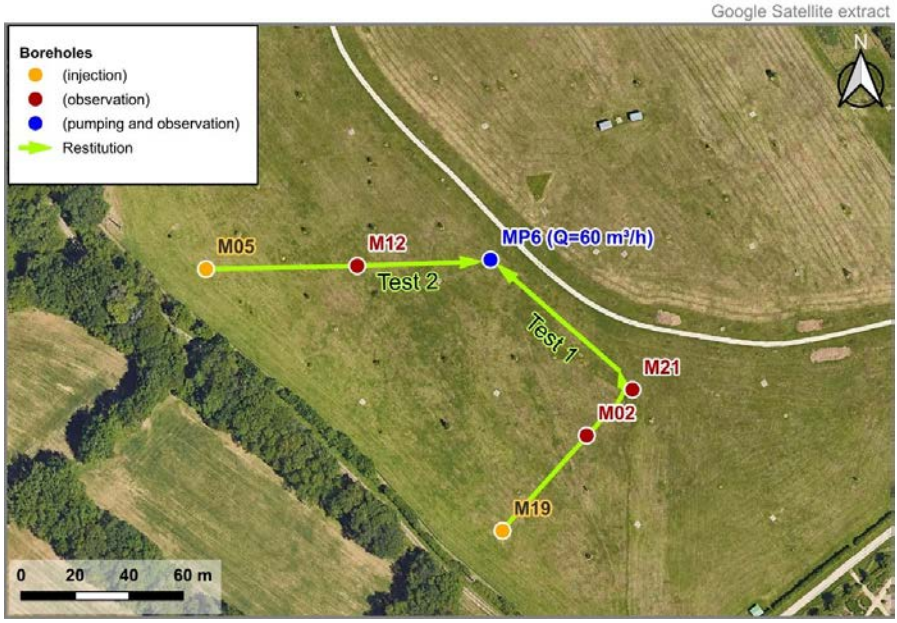

Figure 16 *Location of the boreholes MP6 (pumping and observation) M05 (injection) M19 (injection) and observation wells (M02, M12, M21).*

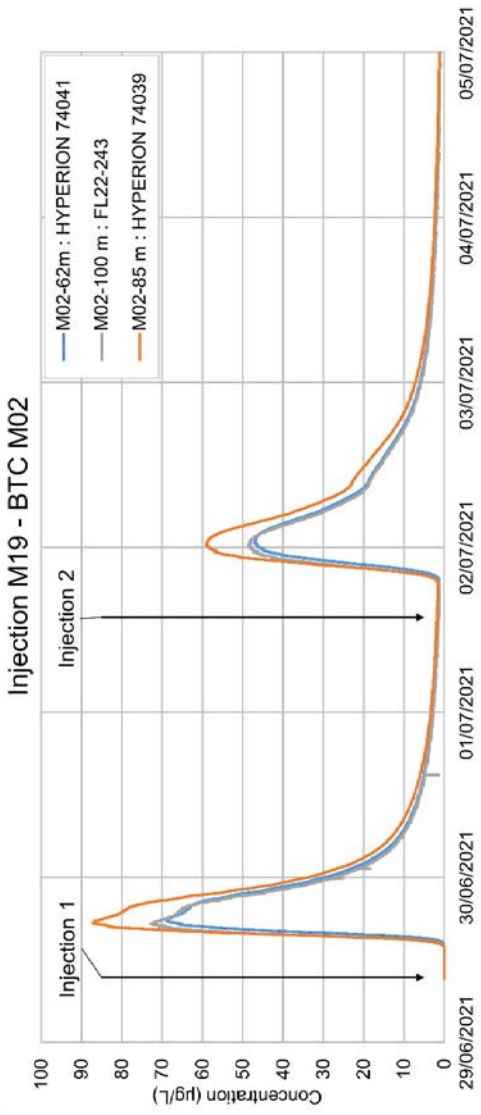

Figure 17 *Experimental BTC M02 after injections into M19.*

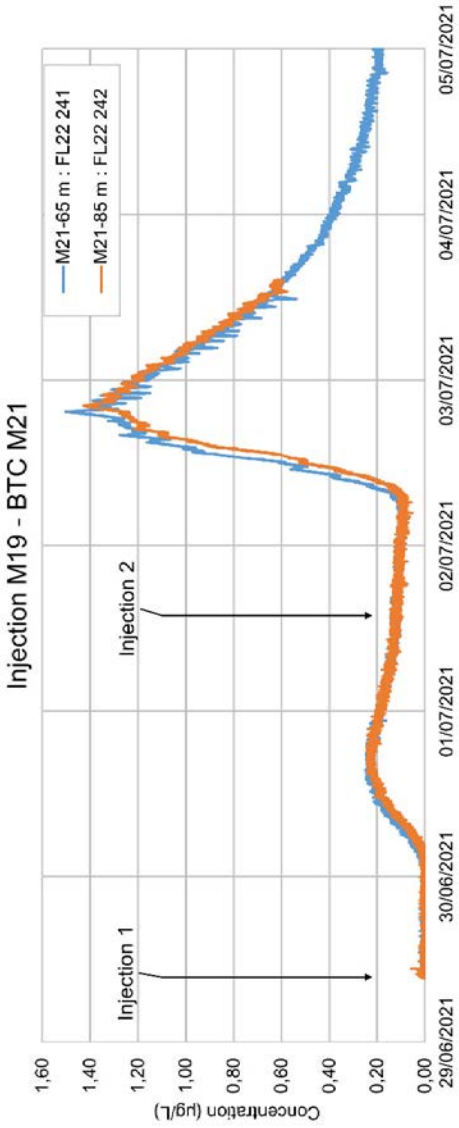

Figure 18 *Experimental BTC M21 after injections into M19.*

The BTC obtained following the injection carried out on M05 at 111 m depth is reported in Figure 19. The arrival times of the first concentration and the concentration peaks made it possible to confirm an upward flow in the M12 observation borehole.

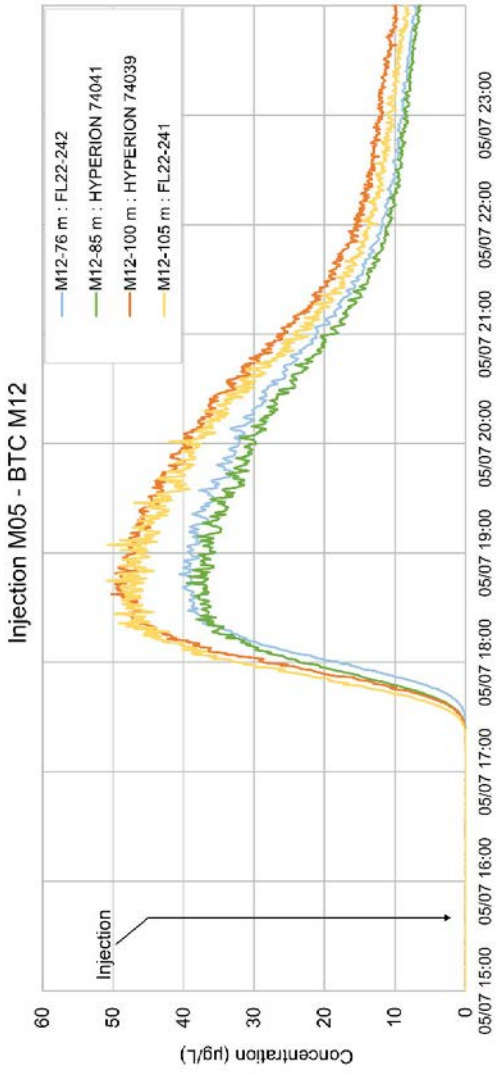

Figure 19 *BTC experimental M12 after injection in M05.*

Conclusion and interpretation of pathways in karst horizons

In addition to the flow log results, the tracer tests provide further clarification of mass transfers within the boreholes, in relation to the porous and karstic levels intersected between 35 m and 115 m, as defined by geophysical and GFTC logs (Tab. 1). The results are presented in Figures 20 and 21.

The tracer responses indicate ascending flows in M02 and M12, and descending flows in M21 (Fig. 20). The boreholes drilled on the experimental site thus act as conduits connecting the karst levels and appear to be solely responsible for the

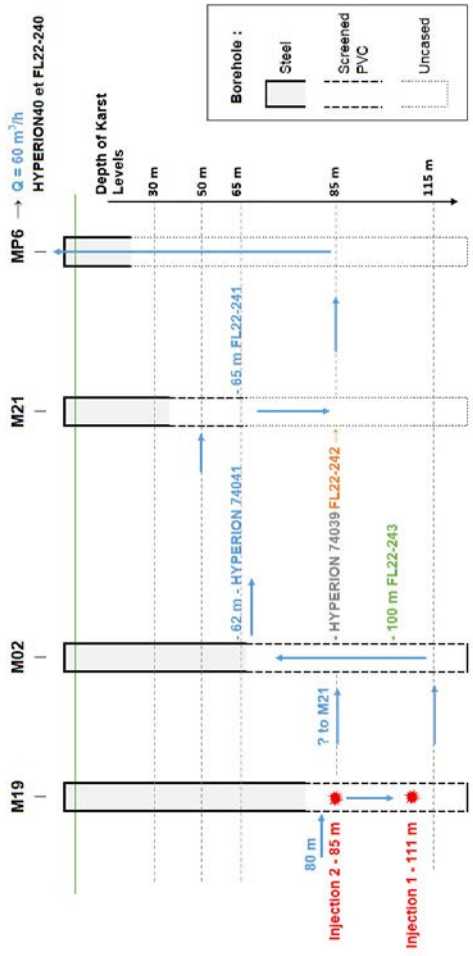

Figure 20 *Hydrogeological cross-section from M19 to MP6.*

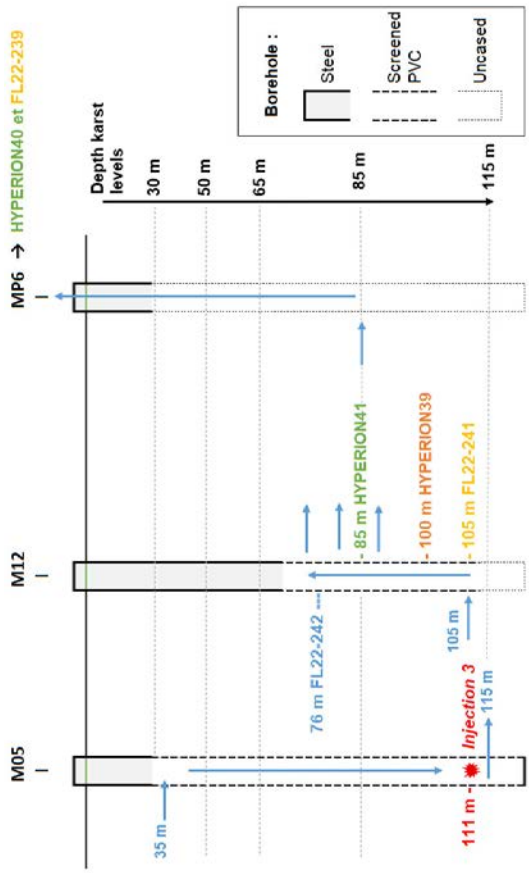

Figure 21 *Hydrogeological cross-section from M05 to MP6.*

observed mass transfers. These transfer fluxes are consistent with the borehole flow results obtained during pumping tests on MP6 (Fig. 4).

Furthermore, the stratified organization of karst conduits is corroborated by field observations of rock outcrops located a few kilometres from the HES, within the same lithostratigraphic horizons (Gaillard et al., 2024).

References

Audouin O., Bodin J., Porel G., Bourbiaux B. (2008). Flowpath structure in a limestone aquifer: multi-borehole logging investigations at the hydrogeological experimental site of Poitiers, France, *Hydrogeology Journal*, 16: 939-950. https://doi.org/10.1007/s10040-008-0275-4

Bodin J., Porel G., Nauleau B., Paquet D. (2022). Delineation of discrete conduit networks in karst aquifers via combined analysis of tracer tests and geophysical data, *Hydrology and Earth System Sciences*, 26 (6): 1713-1726. https://doi.org/10.5194/hess-26-1713-2022

Castany J., Margat J. (1977). Dictionnaire français d'hydrogéologie (French dictionary of hydrogeology). BRGM Ed.

Gaillard T., Moreau M., Mari J.-L. (2024). Seismic and stratigraphic characterization of karstogenic horizons in a sequence of carbonate deposits: Example of the Dogger limestones of the Poitou threshold. In E3S Web of Conferences, Volume 504 (2024) Journées Scientifiques AGAP Qualité 2024, Poitiers, France, 26 au 28 mars 2024, Published online: 26 March 2024, Published online: 26 March 2024. https://doi.org/10.1051/e3sconf/202450405005

Gaillard T., Moreau M. (2026). "Hydrogeology of the Poitou Threshold", Chapter 3 in *A new concept of karst development based on hydrogeology and geophysics*, EDP Science, https://doi.org/10.1051/978-2-7598-3934-6.c003

Keys W.S. (1990) Borehole geophysics applied to ground-water investigations. Techniques of Water Resources Investigations, book 2, chapt. E-2, US Geological Survey, Reston, VA.

Mangin A. (1975). Contribution à l'étude hydrodynamique des aquifères karstiques, troisième partie: constitution et fonctionnement des aquifères karstiques [Contribution to the hydrodynamic study of karst aquifers, part three: constitution and functioning of karst aquifers]. *Annales de spéléologie*, 30(1): 21-124.

Mari J.-L., Porel G. (2008). 3D Seismic Imaging of a Near-Surface Heterogeneous Aquifer: A Case Study. *Oil & Gas Science and Technology (IFP)*, 63(2): 179-201. https://doi.org/10.2516/ogst:2007077

Mari J.-L., Porel G., Bourbiaux B. (2009). From 3D Seismic to 3D Reservoir Deterministic Model Thanks to Logging Data: the Case Study of a Near Surface Heterogeneous Aquifer. *Oil & Gas Science and Technology (IFP)*, 64(2): 119-131. https://doi.org/10.2516/ogst/2008049

Mari J.-L., Porel G. (2024). "The Hydrogeological Experimental Site of Poitiers: Hydrogeological versus geophysical investigations", In *E3S Web of Conferences* 504, Journées Scientifiques AGAP Qualité 2024, Poitiers, France, 26 au 28 mars 2024, Published online: 26 March 2024. https://doi.org/10.1051/e3sconf/202450405003

Muldoon M.A., Simo J.A.T., Bradbury K.R. (2001) Correlation of hydraulic conductivity with stratigraphy in a fractured-dolomite aquifer, northeastern Wisconsin, USA. *Hydrogeol J.*, 9: 570-583. https://doi.org/10.1007/s10040-001-0165-5

Nauleau B., Porel G., Paquet D., Battais A., Bodin, J. (2022). Technical specifications of the boreholes at the Hydrogeological Experimental Site (HES) of Poitiers, France, French National Observatory HC, https://doi.org/10.26169/hplus.poitiers_technical_logs

Paillet F.L. (1993). Using borehole geophysics and cross-borehole flow testing to define hydraulic connections between fracture zones in bedrock aquifers. *J. Appl. Geophys.*, 30: 261-279.

Paillet F.L., Reese R.S. (2000) Integrating borehole logs and aquifer tests in aquifer characterization. *Ground Water*, 38: 713-725.

Schürch M., Buckley D. (2002) Integrating geophysical and hydrochemical borehole log measurements to characterize the Chalk aquifer, Berkshire, United Kingdom. *Hydrogeol. J.*, 10: 610-627.

Williams J.H., Lane J.W., Singha K., Haeni F.P. (2002) Application of advanced geophysical logging methods in the characterization of a fractured-sedimentary bedrock aquifer, Ventura County, California. US Geol Surv. Water Resour Invest Rep 00-4083.

Worthington S.R.H. (2003). A comprehensive strategy for understanding flow in carbonate aquifers. Speleogenesis and Evolution of Karst Aquifers 1 (1), www.speleogenesis.info, re-published from: Palmer, A.N., Palmer, M.V., and Sasowsky, I.D. (eds.), 1999. Karst Modeling: Special Publication 5, The Karst Waters Institute, Charles Town, West Virginia (USA): 30-37.